Contributions of the synoptic meteorology to the seasonal CCN cycle over the Southern Ocean

Tahereh Alinejadtabrizi[1,2,3], Yi Huang[3,4], Francisco Lang[1,5], Steven Siems[1,2], Michael Manton[1], Luis Ackermann[6], Melita Keywood[7,8], Ruhi Humphries[7,8], Paul Krummel[7], Alastair Williams[9], and Greg Ayers[10]

[1]School of Earth, Atmosphere and Environment, Monash University, Melbourne, Victoria, Australia
[2]Australian Research Council Securing Antarctica's Environmental Future (SAEF), Melbourne, Victoria, Australia
[3]Australian Research Council Centre of Excellence for Climate Extremes (CLEX), Melbourne, Victoria, Australia
[4]School of Geography, Earth and Atmospheric Sciences, The University of Melbourne, Melbourne, Victoria, Australia
[5]Department of Geophysics, Universidad de Concepción, Concepción, Chile
[6]Australian Bureau of Meteorology, Melbourne, Victoria, Australia
[7]CSIRO Environment, Melbourne, Victoria, Australia
[8]Australian Antarctic Program Partnership, Institute for Marine and Antarctic Studies, University of Tasmania, Hobart, Tasmania, Australia
[9]Environmental Research, ANSTO, Lucas Heights, New South Wales, Australia
[10]Visiting Scientist Emeritus, Bureau of Meteorology, Melbourne, Victoria, Australia

Correspondence: Tahereh Alinejadtabrizi (tahereh.alinejadtabrizi@monash.edu)

Abstract. Cloud Condensation Nuclei (CCN) play a fundamental role in determining the microphysical properties of low- level clouds, crucial for defining the energy budget over the Southern Ocean (SO). However, many aspects of the CCN budget over the SO remains poorly understood, including the role of the synoptic meteorology. In this study, we classify six distinct synoptic regimes over the Kennaook/Cape Grim Observatory (CGO) and examine their influence on the seasonal cycle of the CCN concentration (N_{CCN}). Three 'winter' regimes are dominant when the subtropical ridge (STR) is strong and centred at lower latitudes, while three 'summer' regimes prevail when the STR shifts to higher latitudes. Distinct winter and summer 'baseline' synoptic patterns contribute to the seasonal cycle of N_{CCN} with the winter baseline regime characterised by heavier precipitation (0.33 vs 0.10 mm hr^{-1}), a deeper boundary layer (850 vs 900 hPa) and lower N_{CCN} (71 vs 137 cm^{-3}) than the summer one. Across these two baseline regimes we observe a significant inverse relationship between precipitation and N_{CCN}, underscoring the contribution of precipitation in reducing N_{CCN} over the SO. An analysis of air mass back trajectories, specifically at the free troposphere level, supports this seasonal distinction, with wintertime air masses originating more frequently from higher latitudes. The summertime STR is seen as a barrier to Antarctic air masses reaching the latitude of CGO. Conversely, the summer baseline regime is found to pass more frequently over continental Australia before reaching CGO, consistent with enhanced radon concentrations.

1 Introduction

Low-altitude clouds, frequently found in or near the marine atmospheric boundary layer (MABL), are prevalent over mid-latitude oceans (Wood, 2012) and are a pivotal component of the Earth's climate system due to their direct impact on both the energy budget and hydrological cycle (Trenberth and Fasullo, 2010; Williams et al., 2013; Bodas-Salcedo et al., 2014; Tan et al., 2016; Schuddeboom and McDonald, 2021). These clouds are not only notoriously difficult to simulate accurately within climate models (Forbes and Ahlgrimm, 2014; Kay et al., 2016) but also exhibit a profound impact on climate sensitivity of these simulations, especially over the Southern Ocean (SO), as highlighted in the latest phase of the Coupled Model Intercomparison Project (CMIP6) (Zelinka et al., 2020). The radiative properties of these clouds are highly sensitive to both their macrophysics and microphysics (Wood, 2012; Wood et al., 2012), such as cloud droplet number concentration (N_d). Evidence from the Southern Ocean Clouds, Radiation, Aerosol Transport Experimental Study (SOCRATES) emphasized the intimate connection between N_d, cloud condensation nuclei concentrations (N_{CCN}), and aerosol properties in this region. Such insights highlight the critical role of aerosols, particularly cloud condensation nuclei (CCN), in shaping cloud properties and radiative effects over the SO (McFarquhar et al., 2021) and the complex interplay between aerosols, cloud formation, precipitation and the local dynamics and thermodynamics of the MABL.

The N_{CCN} over the SO has been studied for decades (e.g., Gras, 1990, 1995; Ayers et al., 1997; Gras and Keywood, 2017; Humphries et al., 2021) due to its importance and the availability of long-term, high-quality field observations. Located at the northwest tip of Tasmania (40°41'S, 144°41'E), the kennaook/Cape Grim Baseline Air Pollution Station (CGO) has been providing unique access to pristine air masses off the SO during 'baseline' conditions (Gras and Keywood, 2017; Humphries et al., 2023) since 1976. It is worth noting that, henceforth, the term "pristine" refers to air masses with low N_{CCN}. This programme is the principal Australian contribution to the World Meteorological Organization (WMO) Global Atmosphere Watch (GAW) (Gras and Keywood, 2017). From the earliest observations, the CGO record has revealed a robust seasonal cycle in N_{CCN} (Bigg et al., 1984; Ayers et al., 1997; Gras and Keywood, 2017; Humphries et al., 2023). During the austral winter (JJA), the N_{CCN} is at a minimum while peaks are observed over the summer months (DJF).

Dimethylsulphide (DMS), primarily originating from planktonic algae in seawater, emerges as a substantial source of CCN over oceanic regions (Charlson et al., 1987). While marine biological sources predominantly govern N_{CCN} during the summer months, multiple elements, such as sea salt particles produced from sea spray and bubble bursting, contribute to CCN levels throughout the year over the SO (e.g., Ayers and Cainey, 2007; Korhonen et al., 2008; Quinn and Bates, 2011; Hudson et al., 2011; Quinn et al., 2014; Sanchez et al., 2018; Twohy et al., 2021). Beyond these primary contributors, various other sinks (e.g. coalecence scavenging) and sources (e.g. secondary particles) influence the CCN budget over the SO (e.g., Vallina et al., 2006; Fossum et al., 2018; Humphries et al., 2023; Niu et al., 2024), some of which have not been as extensively studied.

Early simulations of the CCN budget within the SO MABL were driven by the CGO record (Ayers et al., 1995), demonstrating the importance of the seasonality of the biogenic activity within the surface fluxes. Such simulations were arguably limited, as a complete 1-D CCN budget of the MABL not only needs surface sources but must also include entrainment from the free

troposphere as a potential source (Clarke et al., 1998; Capaldo et al., 1999; Katoshevski et al., 1999; Jimi et al., 2007; Wood et al., 2012; Rose et al., 2017). Since new particle formation is rare in the MABL (Bates et al., 1998), the exchange with the free troposphere can supply particles that grow into CCN (Korhonen et al., 2008; Williamson et al., 2019; Sanchez et al., 2021). Further, such simple budget models need to include the sink terms from coalescence scavenging and wet deposition (Feingold et al., 1996; Mechem et al., 2006; Wood, 2006; Kang et al., 2022; Alinejadtabrizi et al., 2024), although no such observations have routinely been available. Kang et al. (2022), employing the SOCRATES campaign over the SO along with a simplified but more comprehensive budget model (developed initially by Wood et al. (2012)), highlighted entrainment from the free troposphere as a crucial source during the summertime and coalescence scavenging as a key sink of CCN over the SO (Sanchez et al., 2021). Painemal et al. (2023) also investigated the influence of distinct synoptic patterns dominant over the western North Atlantic during wintertime, demonstrating the critical role of synoptic meteorology in regulating aerosol–cloud–meteorology interactions. Their findings highlight how variations in atmospheric regimes impact cloud microphysics, boundary layer dynamics, and N_{CCN}, emphasizing the importance of accounting for synoptic-scale influences when interpreting CCN variability and aerosol–cloud interactions in extratropical regions.

Examining baseline air masses, Alinejadtabrizi et al. (2024) established a relationship between the N_{CCN}, the cloud morphology, the precipitation, and the synoptic meteorology. Mesoscale cellular convection (MCC) is commonly observed across these latitudes (Danker et al., 2022; Lang et al., 2022, 2024) with open MCC more common during winter. Alinejadtabrizi et al. (2024) established that lower concentrations of CCN coincided with the occurrence of open MCC and relatively heavier precipitation rates in comparison to when closed MCC was observed upwind of CGO. The mean precipitation rate for open MCC was six times greater than for closed MCC, underscoring the importance of wet deposition in removing CCN from the MABL during baseline conditions. This research suggests that the seasonality in the synoptic meteorology may be contributing to the observed seasonal cycle in N_{CCN} through the sink associated with the precipitation rate.

Located at 41°S, the seasonal cycle of the meteorology governing CGO, reflects the annual advance and retreat of the Hadley cell and subtropical ridge (STR) (e.g., Pittock, 1973; Dima and Wallace, 2003; Larsen and Nicholls, 2009; Cai et al., 2011). Defined by the mean latitude and intensity of high-pressure systems near the midlatitudes, the STR is highly correlated to both seasonal rainfall and wind patterns (Larsen and Nicholls, 2009; Grose et al., 2015) and temperatures (Pepler et al., 2018) across Australia. Mace and Avey (2017) documented a seasonal cycle in the meteorology, specifically cloud properties and precipitation processes in warm clouds, over the SO using the A-Train satellite data (consistent with other works e.g., Boers et al. (1998); McCoy et al. (2014, 2015); Huang et al. (2015); Fletcher et al. (2016); Lang et al. (2018, 2022, 2024)).

Moving beyond the biogenic production of DMS, our investigation aims to extend our understanding of the role of the synoptic meteorology in shaping the observed seasonal cycle in the N_{CCN} over CGO under baseline conditions. Specifically, we seek to better appreciate the role of the synoptic meteorology in defining both the seasonal precipitation and free troposphere transport of aerosols. Employing a K-means clustering algorithm, we first define the synoptic meteorology over CGO, which includes separate clusters for wintertime and summertime baseline conditions. Observations of precipitation underscore the significant role of wet deposition as a sink term contributing to the observed seasonality. Using back trajectories for these synoptic clusters,

we also examine the seasonality in air mass origin of the free troposphere transport across the SO. Using radon observations as a proxy for terrestrial influences, we find further evidence of meteorological controls in defining the CCN budget. Finally, the analysis revealed that the STR acts as a seasonal barrier, modulating the connectivity between mid and higher latitudes, which in-turn, can influence the observed air mass characteristics at CGO.

2   Data and Methodology

The meteorological data set is taken from the fifth generation of European ReAnalysis (ERA5), produced by the European Centre for Medium-Range Weather Forecasts (ECMWF) (Hersbach et al., 2020) which is available through the Copernicus Climate Change Service Climate Data Store (https://cds.climate.copernicus.eu). Our analysis employs 8036 virtual soundings taken twice per day (00:00 and 12:00 UTC) over a period of 11 years (2011-2021) over the grid point nearest to CGO.

A simple K-means clustering algorithm (Anderberg, 1973) is employed to classify the 11 years of synoptic meteorology based on the low-altitude thermodynamic structure. K-means clustering algorithm has been widely utilized over the SO to investigate cloud regimes (e.g., Gordon and Norris, 2010; Haynes et al., 2011; Mason et al., 2014), the climatology of MABL (Truong et al., 2020, 2022) and MABL's responses to synoptic forcing (e.g., Hande et al., 2012; Lang et al., 2018; Montoya Duque et al., 2022, 2023). Consistent with the approach of Lang et al. (2018); Truong et al. (2020), a set of 15 variables is employed for the clustering analysis. These include four variables (the temperature, relative humidity, zonal and meridional winds) at the three different atmospheric levels (925, 850, and 700 hPa) and three surface variables (pressure, air temperature and relative humidity). Standardization is applied to each variable before clustering. Initially, the analysis considers the number of the clusters (K) ranging from 2 to 10 (results not shown). Ultimately, 6 clusters were chosen as it represents the minimum number of clusters that effectively differentiates the synoptic meteorology.

To provide further environmental context for each cluster, Estimated Inversion Strength (EIS), which reflects the strength of the boundary layer inversion was calculated. Following the Wood and Bretherton (2006), EIS is defined as

$$EIS = LTS - \Gamma_m^{850}(z_{700} - LCL)$$

where LTS is the lower tropospheric stability, defined as the difference in potential temperature between the 700 hPa level and the surface ($LTS = \theta_{700} - \theta_{surf}$) (Klein and Hartmann, 1993), and Γ_m^{850} is the moist-adiabatic potential temperature gradient at 850 hPa. z_{700} is the altitude of the 700 hPa level and LCL is the lifting condensation level. Total Column Water Vapour (TCWV) or total precipitable water is also used as an indicator for assessing atmospheric moisture content and estimating potential precipitation.

Hourly observations of CCN spanning eleven years are available from the CGO, located at the northwest tip of Tasmania. The particle measurements at CGO, initiated in the mid-1970s with a range of technologies, align with the recommendations of the World Meteorological Organisation's Global Atmosphere Watch (WMO-GAW) programme under the Aerosol Programme (Gras and Keywood, 2017; Humphries et al., 2023). This study utilizes the N_{CCN} at 0.5% supersaturation (Model CCN-100,

Droplet Measurement Technologies, Longmont, CO, USA) for the same twice-daily 8036 soundings. CCN data for other supersaturation levels are not available at these times. Data can be accessed through the World Data Centre for Aerosols (http://www.gaw-wdca.org/). Additionally, hourly measurements of radon, as an unequivocal tracer of terrestrial influences on sampled air masses (Zahorowski et al., 2013; Chambers et al., 2015, 2018), are conducted using a dual-flow-loop two-filter atmospheric radon detector over the CGO station (Whittlestone and Zahorowski, 1998; Williams and Chambers, 2016). The hourly precipitation data, in $\mathrm{mm\,hour^{-1}}$, were also obtained from the Australian Bureau of Meteorology rain gauge stationed close to CGO (Station ID: 091331) for the corresponding times. The detection threshold of rain gauge is 0.2 mm. Over the 11-year period of interest, precipitation is recorded only 12% of the time, while 88% of the time the precipitation was recorded to be 0 mm. Due to this high occurrence of non-precipitating conditions, the median precipitation value is zero, necessitating the use of the mean precipitation value for analysis, unlike the N_{CCN} where the median was used. These observations also highlight the nature of precipitation over our study area where it often experiences intermittent precipitation, which may occur within one hour followed by dry conditions in the next. This variability is consistent by the dominance of both open and closed MCCs over the region (e.g., Alinejadtabrizi et al., 2024).

Traditionally for CGO, the baseline sector is defined as periods with surface wind directions between 190° and 280° (Ayers and Gillett, 2000; Gras et al., 2009), coupled with radon concentrations below various thresholds such as 150 mBq m^{-3} (Gras and Keywood, 2017). No distinction is made for season. We define this constraint as "CGO baseline" hereafter, as opposed to the "Winter baseline" and "Summer baseline" clusters produced from our cluster analysis. Air sampled in the CGO Baseline sector has typically traversed several thousand kilometres across the SO, with minimal recent anthropogenic and terrestrial influences (Ayers and Gillett, 2000; Gras and Keywood, 2017).

The Hybrid Single Particle Lagrangian Integrated Trajectory (HYSPLIT) model was employed for running the back trajectories (Draxler and Hess, 1998), to analyze the source of the air parcels, along with the hourly ERA5 data served as the input for meteorological parameters.

3 Synoptic classification

The application of the K-means clustering algorithm (K = 6) to the 11 years of ERA5 atmospheric profiles (twice per day) over CGO has revealed distinct synoptic patterns that vary seasonally. The mean sea level pressure (MSLP) composite plots for these six clusters (Figure 1) demonstrate a clear division into two groups based on the location of high-pressure centers. The top row in Figure 1 shows three clusters with high-pressure centers located over lower latitudes, and the bottom row features three clusters with high-pressure centers positioned over higher latitudes. This distinction will be examined in greater detail later in this section.

Further distinctions are noted by the column. In the left-hand column (Figures 1a and d), the MSLP contours are aligned from southwest to northeast near CGO (highlighted by star sign in Figure 1), with wind vectors oriented from the southwest toward the station. This configuration indicates that CGO predominantly experiences a south-westerly or baseline air mass

145 in these clusters. In contrast, the middle column (Figures 1b and e) displays MSLP contours and wind vectors oriented from northwest to southeast, suggesting a continental influence on the air mass. The right-hand column (Figures 1c and f) shows clusters where CGO is located near high-pressure centers with weak surface winds. Based on these observations, the clusters are initially categorized into three synoptic groups: Baseline (characterized by baseline air masses from higher latitudes), Frontal (influenced by continental air masses from the northwest), and High-Pressure (associated with weak surface winds

150 near high-pressure centers).
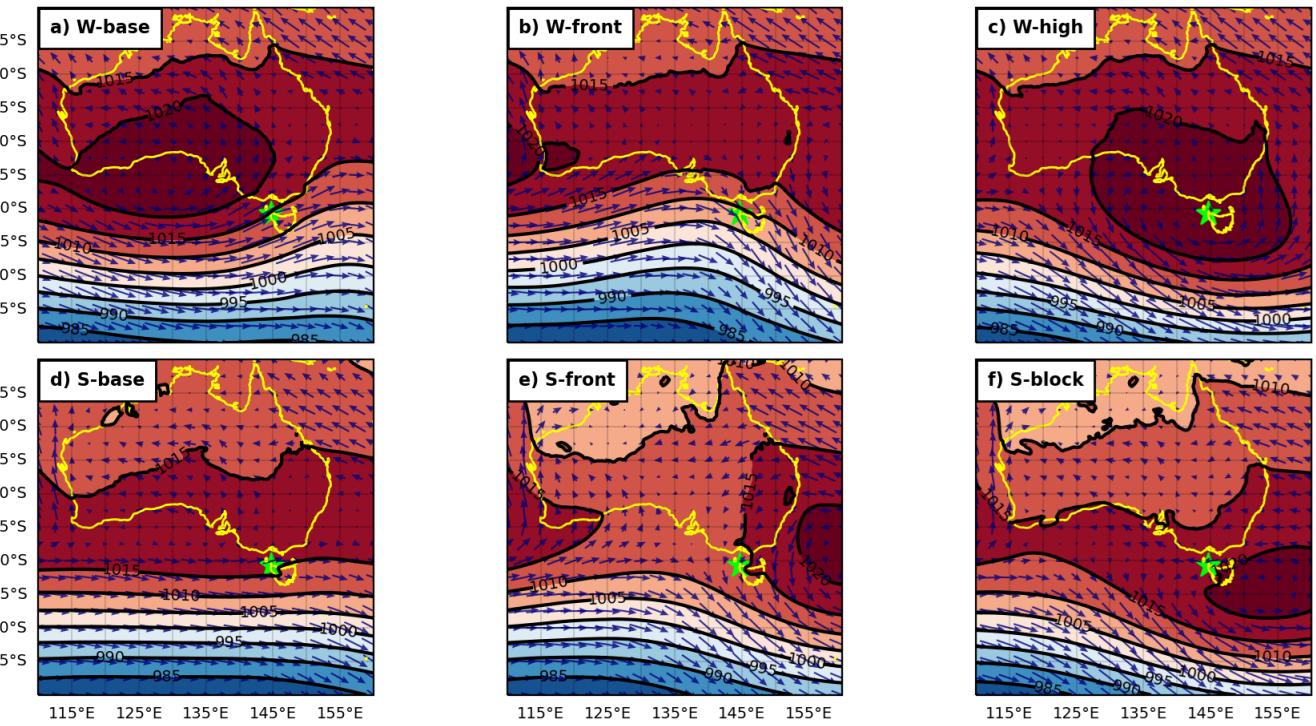
Figure 1. MSLP composite for six synoptic clusters: a. winter baseline (W-base), b. winter frontal (W-front), c. winter high-pressure (W-high), d. summer baseline (S-base), e. summer frontal (S-front) and f. summer blocking (S-block) (2011-2021). The dark blue wind vectors (at 10m) overlaid. The star symbol highlights the location of CGO.

To further explore the differences between the three main synoptic groups identified earlier (between the columns), we examine the frequency of occurrence of each cluster throughout the year (Figure 2a). Three clusters, shown in blue, exhibit higher frequencies during the austral winter months (June, July, August, and September), while the other three, shown in red, are more prevalent during the austral summer months (December, January, February, and March). To simplify interpretation, the

155 clusters are further grouped into two seasonal categories: Winter Clusters (names starting with 'W') and Summer Clusters (names starting with 'S'). Throughout all figures, winter clusters are represented in blue/top row and summer clusters in

red/bottom row. It should be noted that due to the inherent variability of the synoptic meteorology, some data points from winter may be classified within the summer clusters and vice versa.
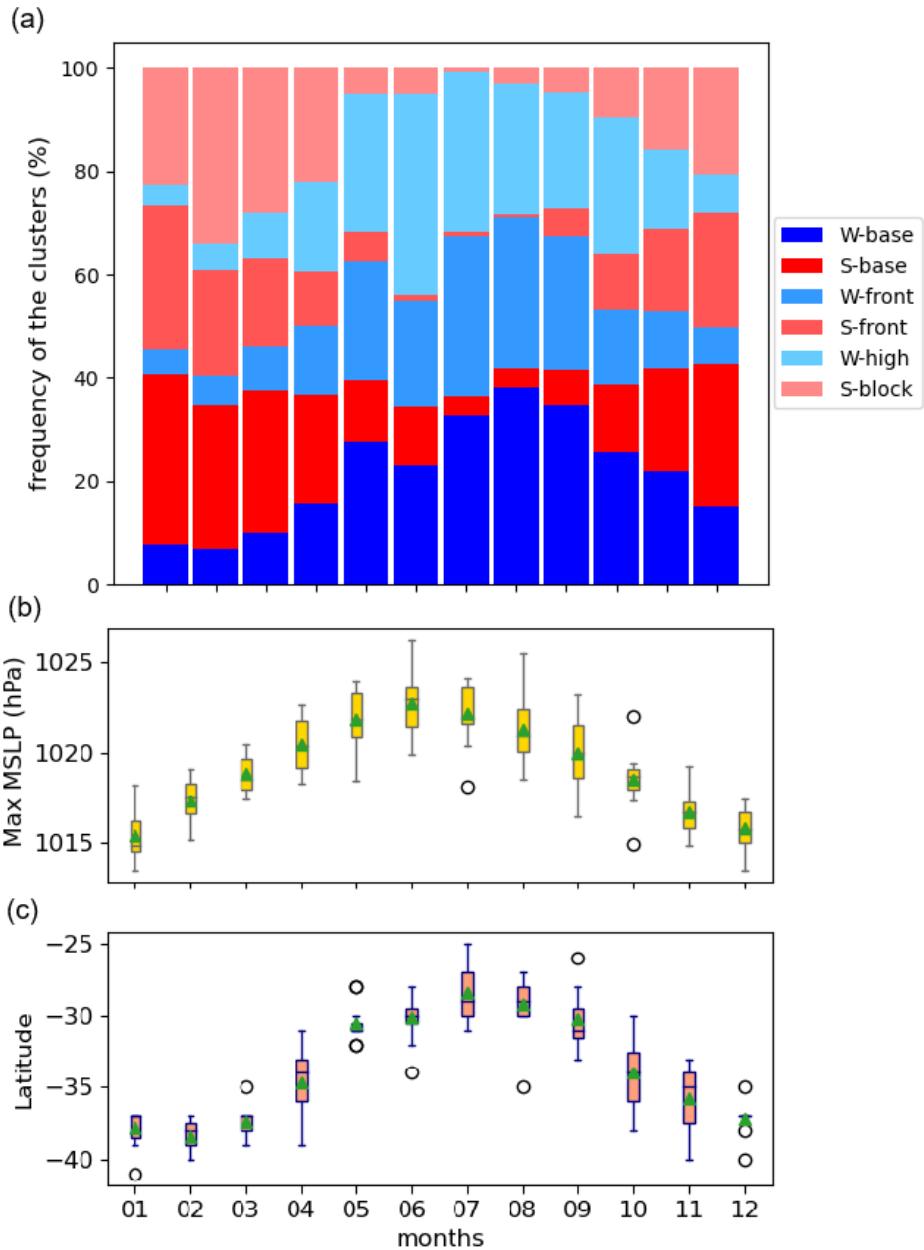
Figure 2. Observed seasonality in: a. the frequency of appearance of the 6 clusters, b. the maximum MSLP (intensity) itself and c. the latitude where the maximum MSLP occurs (2011-2021). The green triangles in the Box-whisker plots represent the mean values, the middle line inside the boxes represents the median and the top and bottom of the boxes indicate the 25th and 75th percentiles. Hollow circles denote outliers.

To better understand the observed seasonality, we analyze the location and intensity of the Subtropical Ridge (STR) using MSLP data from ERA5, covering the same 11-year period (twice daily). Zonal MSLP values were calculated for each latitude between 10–60°S, spanning longitudes from 110–160°E for each month. Then the maximum MSLP (intensity) and its latitude of occurrence were determined, as shown in Figures 2b and c, respectively. Figure 2c illustrates the well-documented annual progression of the STR over our 11-year study period, migrating to lower latitudes during the austral winter (JJA) and higher latitudes in the austral summer (DJF). This behavior aligns with established literature (e.g., Williams and Stone, 2009; Larsen and Nicholls, 2009). Figure 2b shows that as the STR shifts equatorward, its maximum pressure increases, while lower pressures are observed during summer when the STR is located further poleward, which is again consistent with the findings of Larsen and Nicholls (2009). The seasonal cycles of all six clusters are seen to be highly correlated with the migration of the STR, reflecting the role of the synoptic meteorology in determining the air mass being observed at CGO (Figure 2).

Next, we examine composite soundings for the six clusters using the ERA5 datasets (Figure 3). Starting with the left-hand column (Figure 3a and d), a south westerly wind is observed at the surface, consistent with the composite MSLP plots (Figure 1a and d). The wintertime composite (Figure 3a) has a more southerly heading of the two. As we move from the boundary layer into the free troposphere, the wind direction remains largely unchanged in winter (Figure 3a) but turns more westerly in summer cluster (Figure 3d). The inversion is seen to be deeper in the winter (~850 hPa) (Table B1). Conversely, the inversion is shallower (~900 hPa) for the summer composite (Figure 3d). Again, the 1000 hPa winds align closely with the definition of CGO baseline conditions (e.g., Ayers et al., 1995; Gras and Keywood, 2017; Humphries et al., 2023), support their classification as summertime (S-base) and wintertime (W-base) baseline clusters. We note that the composite W-base sounding is similar to the composite open MCC sounding of Alinejadtabrizi et al. (2024, their figure 2b), while the composite S-base sounding is similar to the composite closed MCC sounding (their figure 2a). Lang et al. (2022) has previously established that open MCC occurs more frequently during the winter in the region up wind of CGO.

The EIS also reflects this pattern, with higher EIS for the S-base (4.3°K for W-base vs. 6.6°K for S-base) indicating more stable conditions (Table B1), which is favourable for the closed MCCs (McCoy et al., 2017). This is consistent with the prevalence of closed MCCs during summer, as noted in the literature (e.g., Lang et al., 2022; Alinejadtabrizi et al., 2024).

Moving to the middle column (Figure 3b and e), a strong north westerly wind is evident through the free troposphere consistent with their classification as frontal clusters, W-front and S-front, respectively. The S-front cluster shows strong turning through the boundary layer. Turning attention to the last two clusters in the right-hand column (Figure 3c and f), they show a relatively pronounced inversion. The cluster which is more common during the winter (Figure 3c) features a relatively deeper inversion at ~900 hPa, where the EIS is 6.3°K. The other cluster (Figure 3f) has an inversion at ~950 hPa with an EIS of 4.7°K (Table B1). The top composite displays zero wind speed consistent with the MSLP composite (Figure 1c), reinforcing the classification of this cluster as a high-pressure system (W-high). The bottom one, on the other hand, illustrates a blocking system commonly observed during the summer season (S-block) (Risbey et al., 2013).
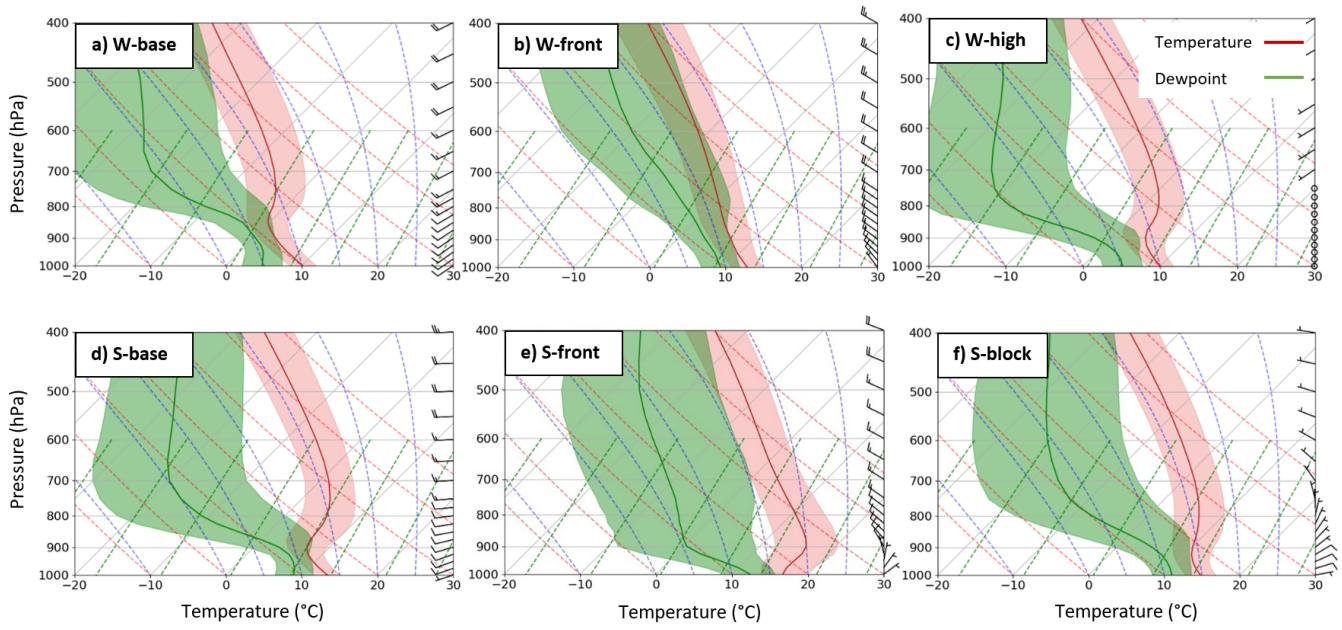
Figure 3. Composite soundings for the six clusters (2011-2021), shaded region indicating 1 standard deviation. Winter clusters are displayed in the top row while the bottom row shows the summer clusters.

In summary a simple K-means clustering has led to the identification of 6 distinct clusters that exhibit specific synoptic and seasonal meteorological characteristics over CGO. The two baseline clusters are most common, combined they occur ~40% of the time. The two frontal clusters occur ~27% of the time combined. Finally, W-high and S-block occur ~33% of the time, combined (more details can also be found in Table 1).

195 The 72 hours back trajectories at boundary layer elevation (500 m) (Figure 4) reveal the history of the air mass being observed at CGO for each of the 6 clusters, largely confirming the synoptic classification. 72 hours has been selected to capture the connectivity between lower latitudes (the continent) and higher latitudes (Antarctica). This time frame also aligns with the typical timescale between cyclones in the Southern Hemisphere (Jimi et al., 2007). The air mass of both baseline clusters (Figure 4a and d) predominantly originates over the SO, suggesting the minimal terrestrial influence. These 2 clusters also

200 display the greatest displacement compared to the other four clusters (with the W-base having the greatest average length of ~3743 km), reflecting the influence of strong westerly winds across the SO storm track. Back trajectories for W-base have a more southerly heading at CGO and are more likely to have originated at higher latitudes, with 22% of these trajectories cross the 60°S latitude, even occasionally reaching Antarctica. The S-base back trajectories have a more westerly heading at CGO with only 2% originating from higher latitudes (crossing 60°S).

205 Back trajectories for both frontal clusters (Figure 4b and e) suggest a likely terrestrial influence on air masses reaching CGO. During the winter, when the STR is furthest north, the back trajectories still commonly originate over the SO, but can loop

over the continent before reaching CGO. Finally, the back trajectories for W-high (Figure 4c) and S-block (Figure 4f) reflect the weak wind speeds near CGO due to smallest spreads during these synoptic conditions.
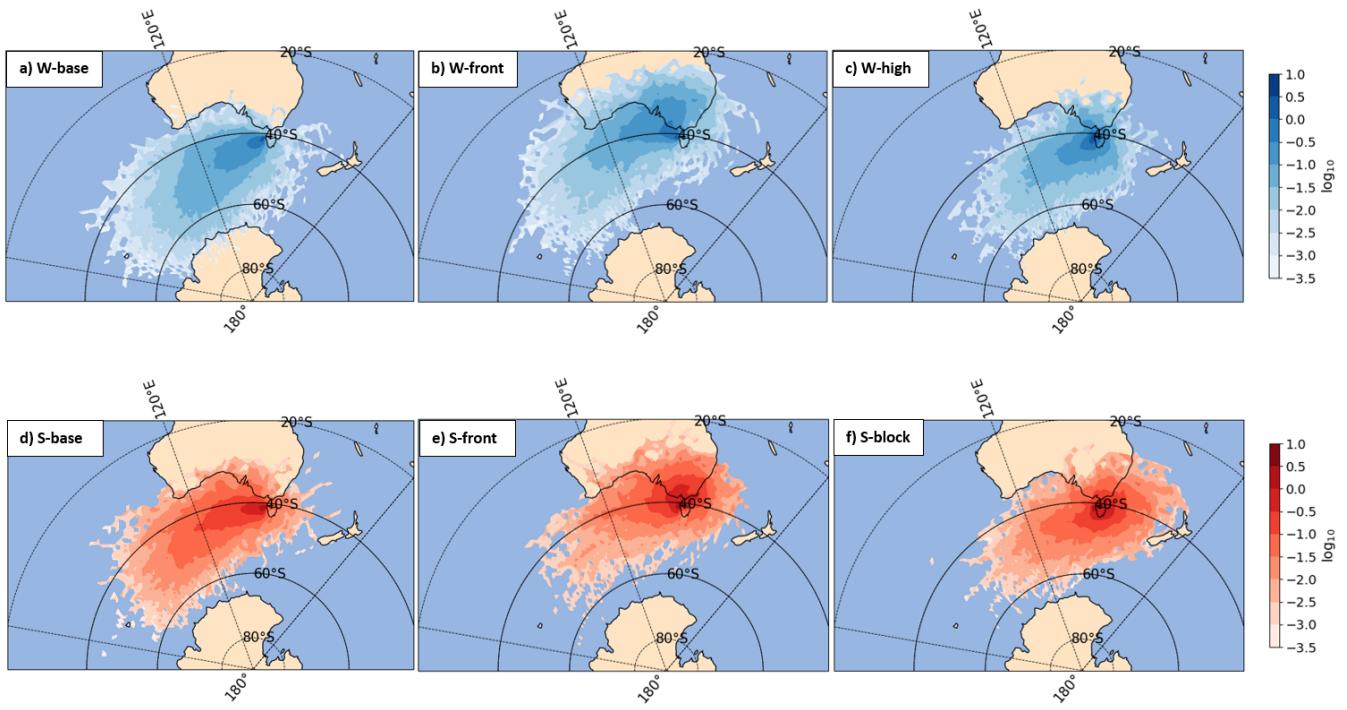
Figure 4. Frequency of the distribution of 72hours back trajectories at the altitude of 500 m (boundary layer) for six clusters (2011-2021).

4 Air mass characteristics

210 Having used the ERA5 reanalysis to define the synoptic meteorology at CGO, we now employ these six synoptic clusters to isolate the influence of the meteorology on the CGO records (Table 1). For each of the six clusters, the median CCN and radon concentrations and mean precipitation intensity and frequency are calculated and discussed in the following sections. We assessed whether these parameters are different between our clusters with the null hypothesis that any differences are only due to random variations. Not surprisingly, W-base is characterised as the most pristine air mass (N_{CCN} 71 cm^{-3}, radon 66 mBq

215 m^{-3}) having the least exposure to terrestrial influences. S-base, which does pass over Australia more commonly, has around twice the concentration of CCN (N_{CCN} 137 cm^{-3}) and higher radon (80 mBq m^{-3}). The differences in the median CCN and radon concentration between these two baseline clusters were found to be statistically significant ($p < 0.05$) using the Whitney U test [1]. Combined, the baseline clusters yield a large seasonal cycle in CCN consistent with previous results (Ayers et al., 1997; Gras and Keywood, 2017; Humphries et al., 2023).

---

[1]This test is suitable for working with the medians

220 Conversely the two frontal clusters are the least pristine, having more than three times greater N_{CCN} than the corresponding baseline clusters. W-front (N_{CCN} 223 cm^{-3}, radon 574 mBq m^{-3}) is still more pristine than S-front (N_{CCN} 662 cm^{-3}, radon 680 mBq m^{-3}) for both the CCN and radon concentration. This aligns with the well established understanding that air mass off the continent carry higher aerosol levels from urban and industrial sources, contributing to elevated N_{CCN} (e.g., Ayers et al., 1982). The differences in N_{CCN} between our two frontal clusters were found to be statistically significant ($p < 0.05$) through the

225 Whitney U test while the difference in radon was not statistically significant ($p = 0.052$). Finally, the two remaining clusters, W-high (N_{CCN} 126 cm^{-3}, radon 197 mBq m^{-3}) and S-block (N_{CCN} 289 cm^{-3}, radon 424 mBq m^{-3}), fall in between the extremes. In this case the differences are both statistically significant ($p < 0.05$). Overall, the combined summer clusters have a higher N_{CCN} and radon concentration than the combined winter clusters.

Table 1. Median CCN and radon concentration along with their 10th and 90th percentile values and the mean precipitation intensity and frequency for the six clusters.

Clusters (2011-2021)	Number of cases from a total of 8036	N_{CCN} (cm^{-3}) (10th,90th)	Radon (mBq m^{-3}) (10th,90th)	Precipitation intensity (mm hour^{-1}) frequency (%)
Winter Baseline (W-base)	1742 (21.7%)	71 (28,164)	66 (35,174)	0.10 18.4
Summer Baseline (S-base)	1388 (17.3%)	137 (47,392)	80 (33,591)	0.03 5.8
Winter Frontal (W-front)	1307 (16.3%)	223 (69,1061)	574 (64,3761)	0.33 30.1
Summer Frontal (S-front)	925 (11.5%)	662 (162,2041)	680 (95,3371)	0.03 4.8
Winter High pressure (W-high)	1535 (19.1%)	126 (36,685)	197 (55,1361)	0.02 3.3
Summer Blocking (S-block)	1139 (14.2%)	289 (98,949)	424 (118,1570)	0.08 6.9

4.1 Precipitation

Overall, we find the precipitation rate and frequency for each of the six clusters to be highly consistent with the composite soundings (Figure 3). The differences in mean precipitation between the clusters were found to be statistically significant using the two-tailed Student's t test [1] ($p < 0.05$). W-front has the greatest precipitation intensity and frequency (0.33 mm hr^{-1}, 30.1%, respectively) consistent with a weak boundary layer inversion (EIS = 1.2°K), a high relative humidity up through the free troposphere (~69%) and also relatively high TCWV (~19.6 mm) (Table B1). Conversely, W-high, which has the smallest precipitation intensity and frequency (0.02 mm hr^{-1}, 3.3%), has a strong (EIS = 6.3°K), shallow boundary layer inversion (~900 hPa), a low relative humidity through the free troposphere (~34%) and a relatively low TCWV (~12.1 mm) (Table B1). S-front, the cluster with the next weakest precipitation intensity and frequency (0.03 mm hr^{-1}, 4.8%), has a relatively strong (EIS = 3.9°K) (Table B1).

A strong seasonal difference in the precipitation is present for the baseline clusters, W-base precipitates (intensity of 0.10 mm hr^{-1} and frequency of 18.4%) at three times the intensity and frequency of S-base (0.03 mm hr^{-1}, 5.8%), having a weaker (EIS of 4.3°K for W-base vs. 6.6°K for S-base), higher boundary layer inversion (~850 hPa for W-base vs. ~900 hPa for S-base) (Figure 3a and d) (Table B1). The higher precipitation frequency and intensity during W-base are consistent with our earlier note of the resemblance between the W-base sounding and that of open MCCs in Alinejadtabrizi et al. (2024, their figure 2b), which exhibited higher precipitation frequency and intensity when present upwind of CGO (Alinejadtabrizi et al., 2024). It is noteworthy that open MCCs are often accompanied by frequent light precipitation or drizzle (Ahn et al., 2017). Overall, higher wintertime precipitation rates are also consistent with the migration of the STR to lower latitudes during the wintertime (Figure 2c). Manton et al. (2020) reported a negative correlation between precipitation and MSLP over the SO.

Focusing on the baseline air masses, we further explore the inverse relationship between precipitation and N_{CCN}. The higher precipitation rate and lower N_{CCN} of W-base is consistent with that proposed by Kang et al. (2022); Sanchez et al. (2021); Alinejadtabrizi et al. (2024) regarding the role of coalescence scavenging and wet deposition in cleansing the atmosphere and reducing N_{CCN}. The apparent negative correlation of precipitation and N_{CCN} is also evident within the two frontal clusters. While W-front and S-front have similar concentrations of radon (574 and 680 mBq m^{-3}, respectively), the S-front N_{CCN} (662 cm^{-3}) is more than three times as great as W-front N_{CCN} (223 cm^{-3}) with the W-front precipitation (intensity of 0.33 mm hr^{-1} and frequency of 30.1%) being an order of magnitude greater than that of S-front (intensity of 0.03 mm hr^{-1} and frequency of 4.8%). In the case of the last two clusters (W-high and S-block), however, we observe higher precipitation in summertime (S-block) coinciding with higher N_{CCN} level. Comparing the back trajectory plots for these clusters (Figure 4c and f), we observe that W-high air masses spend less time over land than those of S-block, presumably acquiring relatively fewer aerosols, on average.

---

[1]This test is appropriate for comparing the mean of different groups
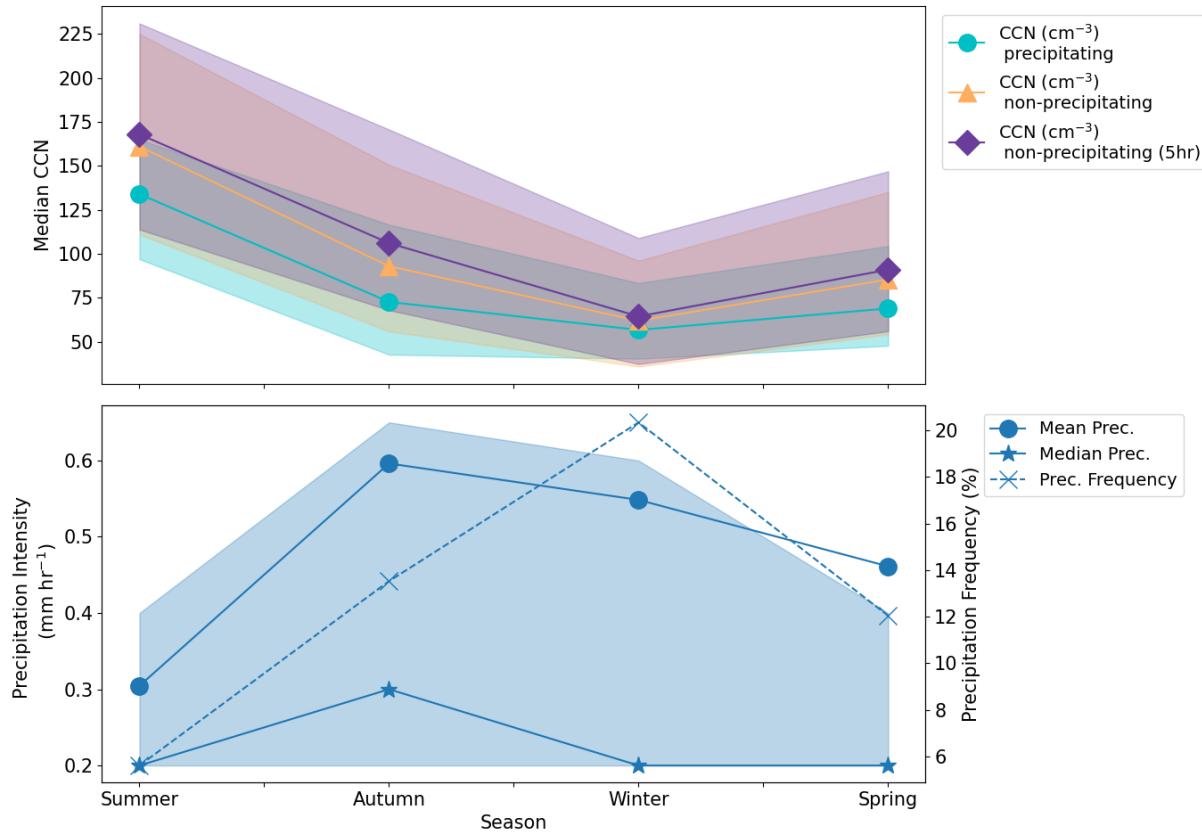
Figure 5. Seasonal cycle of median N_{CCN} (a) along with the mean precipitation intensity and frequency (b) in the two baseline clusters. The shaded area shows the 25th and 75th percentile. Median CCN concentrations are shown separately for precipitating conditions (circles), non-precipitating conditions (triangles), and conditions with no rain during the three preceding hours and no rain in the subsequent hour (diamonds)

Based on the relationships established in the hourly records of the cloud morphology, N_{CCN} and the precipitation rate, and
the seasonality of the cloud morphology (mesoscale cellular convection) upwind of CGO (Lang et al., 2022), Alinejadtabrizi
et al. (2024) hypothesized that a seasonal cycle exists in the baseline precipitation rate at CGO and that wet deposition from
this precipitation contributes to the seasonal cycle in N_{CCN}. Combining these two baseline synoptic patterns (W-base and S-base) returns the historic seasonal cycle in N_{CCN} at CGO (e.g., Gras and Keywood, 2017; Humphries et al., 2023) (Figure
5a) with a peak concentration observed during winter and a minimum over summer. While this approach obscures the role
of the synoptic meteorology, it allows us to examine the seasonal cycle in the baseline precipitation rate at CGO and its
correlation with the seasonal cycle in N_{CCN}. To strengthen the analysis, we further separated N_{CCN} into precipitating and
non-precipitating conditions, enabling a clearer view of the impact of precipitation on N_{CCN}. However, due to the intermittent
nature of precipitation over the study area, cases classified as non-precipitating may still be influenced by precipitation from

preceding or subsequent events. To address this, we introduced a "non-precipitating (5 hr)" condition, defined as hours with
no rain during the three hours prior and no rain in the subsequent hour. While this approach provided a limited subset (1,786
cases) of all non-precipitation hours (2,511 cases), it allowed us to isolate periods with minimal influence by wet deposition.
Figure 5a illustrates the seasonal variation in median N_{CCN} for the combined baseline observations, under precipitating (cyan
circles), non-precipitating (orange triangles), and non-precipitating (5-hour) (purple diamonds) conditions. The mean (circles)
and median (stars) precipitation intensity (for precipitating conditions) and frequency (crosses) are shown on the bottom panel
(Figure 5b). A clear negative relationship between precipitation and N_{CCN} is evident.

This analysis confirms the first part of the hypothesis regarding the seasonal cycle in the baseline precipitation. The frequency
of precipitation is 5.6% in summer (DJF), with a mean intensity of 0.30 mm hr^{-1} and 20.3% in winter (JJA), with a mean
intensity of 0.55 mm hr^{-1}. The strong negative relationship between the baseline precipitation and N_{CCN} and lower N_{CCN} for
the precipitating condition offers further support to the second part of the hypothesis, suggesting that wet deposition contributes
to the seasonal cycle in N_{CCN}. However, while these findings highlight the importance of wet deposition as a potential sink for
N_{CCN}, they do not provide conclusive evidence of its relative contribution to the overall N_{CCN} budget. Other factors, including
biogenic production and sea salt emissions, are likely to play significant roles. Quantifying the relative importance of wet
deposition and coalescence scavenging as sink terms compared to these other processes remains a critical area for future
research, emphasizing the complexity of precipitation processes and the need for further investigation.

4.2 Free troposphere entrainment

While two primary explanations for the observed seasonal cycle of N_{CCN} at CGO are increased biological production in summer
(source dominant) and greater precipitation during winter (sink dominant), another potential source term is the entrainment of
free troposphere air. We note that the baseline radon concentration is significantly higher in summer than winter (Table 1). Since
radon is a well-established tracer of continental air masses and is largely insensitive to precipitation, this seasonal difference
suggests that the summertime baseline air is more likely to have passed over or near continental Australia. Given the significant
positive correlation between radon and N_{CCN} (not shown), we hypothesize that this terrestrial influence could also contribute
to the seasonal difference in baseline N_{CCN}, either directly through surface emissions or through free troposphere entrainment
(Covert et al., 1996).

Kang et al. (2022) identified the role of free troposphere entrainment of CCN from biogenic sources in controlling cloud droplet
number concentration during SOCRATES, which was held during the Austral summer. In contrast, our focus is on the potential
contribution of continental air masses rather than biogenic sources. Previous studies, including ORACLES (ObseRvations
of Aerosols above CLouds and their intEractionS) project, have demonstrated that terrestrial emissions can affect aerosol
concentrations through long-range transport and entrainment processes (Redemann et al., 2020). For example, aerosols from
terrestrial biomass burning or industrial sources have been shown to modulate N_{CCN} even in remote marine environments,
supporting the plausibility of similar processes in our study area. Within this cluster framework, we can also explore the
potential for the entrainment of air from the free troposphere to contribute to the seasonal difference in N_{CCN}.

Figure 6a and b examines the relative differences in the air mass origin between winter and summer baseline conditions at 500 and 2500m, respectively. The 2500 m level is considered part of the free troposphere to ensure the trajectories remain above shallow boundary layer clouds, as indicated by the composite soundings. In this analysis, the logarithm of the frequency of

305 W-base is subtracted from the logarithm of the frequency of S-base. Mathematically, this is the same as taking the logarithm of the ratios of the frequencies. Positive values (red) indicate that summer parcels were more likely than winter parcels to have passed over a given location. This red region is seen to be located over and nearby to continental Australia. Negative values (blue) suggest that wintertime baseline parcels are more likely to have originated over the high latitudes of the SO. This pattern also suggests that the location of the STR plays a role in defining the origin of these air masses.

310 While Figure 6b suggests that there is a potential for any free troposphere entrainment to contribute to the higher surface observations of N_{CCN}, it is inconclusive. For one, the boundary layer air mass is experiencing this same behaviour, we cannot isolate whether any summertime enhancement of N_{CCN} is coming directly from the boundary layer/surface or through the free troposphere. Further, we have no measure of the entrainment and potential cloud processing in connecting the free troposphere air mass to the surface observations. An analysis of the evolution of the altitude of the back trajectories (Figure A1) suggests

315 that air parcels are primarily subsiding as they approach CGO. However, to fully assess the efficiency of entrainment over the CGO, estimation on cloud processing and entrainment are required, but these sub grid scale processes are not captured by ERA5. Ultimately our results suggest that it is more likely for the free troposphere air mass to have been influenced by continental Australia for summertime conditions than wintertime conditions.
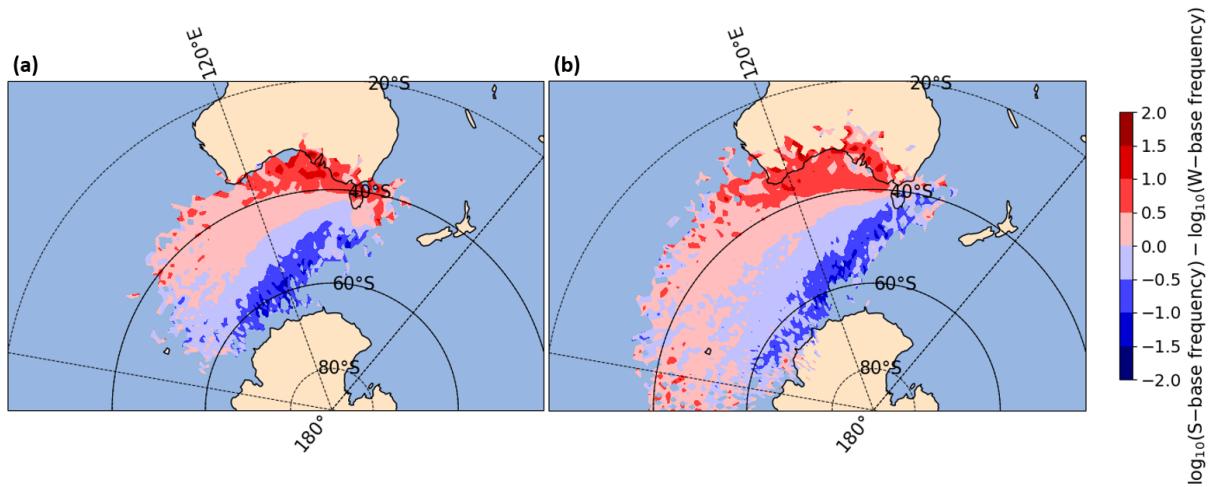
Figure 6. Difference in 72 hours back trajectories between the S-base (red) and W-base (blue) clusters at the a. 500m (boundary layer) and b. 2500m (free troposphere) level.

In an effort to eliminate the potential of direct surface emissions, baseline air parcels were filtered according to their proximity

320 to Australia. If any point of an air parcel's 72 hour back trajectory passed north of 40°S, i.e., gets close to mainland Australia, the air parcel was removed. This filter removed 24% of all W-base hourly records and 55% for S-base. After removing these

air masses that pass close to Australia, there remains a statistically significant difference in N_{CCN} between the 'high-latitude' S-base (122 cm^{-3}) and the 'high-latitude' W-base clusters (71 cm^{-3}). However, no significant difference is observed in their radon concentration (~63 mBq m^{-3}). This suggests that air masses originating from high latitudes are not strongly affected by the entrainment of Australian aerosol sources through the free troposphere, regardless of season. The observed difference in N_{CCN} on the other hand could be attributed to variations in sources, such as biogenic production and the sinks e.g., precipitation.

5 Relationship to CGO baseline air masses

Based on the clusters produced from the ERA5 thermodynamics through the lower free troposphere, we have defined the W-base and S-base clusters. These clusters are independent of the established CGO definition(s) of baseline conditions in the literature. We now explore the consistency between these two different methods of defining baseline (Figure 7). This analysis helps to demonstrate the robustness of our findings with the CGO baseline definitions. Moreover, it highlights the potential significance of synoptic meteorology in understanding baseline conditions.

The primary criterion for CGO baseline is that the local surface wind heading must be between 190°and 280°, i.e., a south-westerly to westerly heading. Over our 11-year record (twice per day), we have 3478 hourly records that meet this criterion using ERA5 winds. We acknowledge that there may be discrepancies between the measured local winds and the ERA5 winds. Of these 3478 hourly records, ~75% are classified as W-base and S-base. Of the remaining 25%, roughly half (12%) come from the W-high cluster. This single criterion for defining baseline is known to be weak with median N_{CCN} at 90 cm^{-3} and radon at 71 mBq m^{-3} (Figure 7a), indicating that continental air masses are being sampled. Looking at this conversely, ~91% of the W-base hourly records and ~76% of the S-base hourly records meet this primary CGO baseline definition. The clustering of ERA5 records is highly consistent with this CGO criterion.

To reduce the influence of terrestrial air masses, it is common for the CGO baseline criteria to be further constrained, removing air masses with high radon concentrations. This radon threshold has become more and more strict over time, reflecting an increasing appreciation of the potential influence of free troposphere entrainment. We have chosen to employ one of the earlier (weaker) radon thresholds of 150 mBq m^{-3}, which still proves to be highly effective, reducing the value of median N_{CCN} from 90 cm^{-3} to 85 cm^{-3} and radon concentration from 71 mBq m^{-3} to 61 mBq m^{-3}. This additional constraint removes nearly 20% of the records. We find that nearly 81% of the remaining 2728 hourly records would now be classified as our baseline clusters (W-base and S-base). The W-high cluster still accounts for over 11% of these records (Figure 7b). Most of the records filtered out by this second threshold came from S-base again highlighting the increased potential for both free troposphere entrainment and direct surface emissions of radon during summer (Figure 7c). It should be noted that a stricter radon threshold (80 mBq m^{-3}) has been examined, and the results (not shown here) indicate that it does not affect the median N_{CCN}. However, the median radon has decreased from 61 to 51 mBq m^{-3}. Also, the percentages of contribution of each cluster do not change significantly.
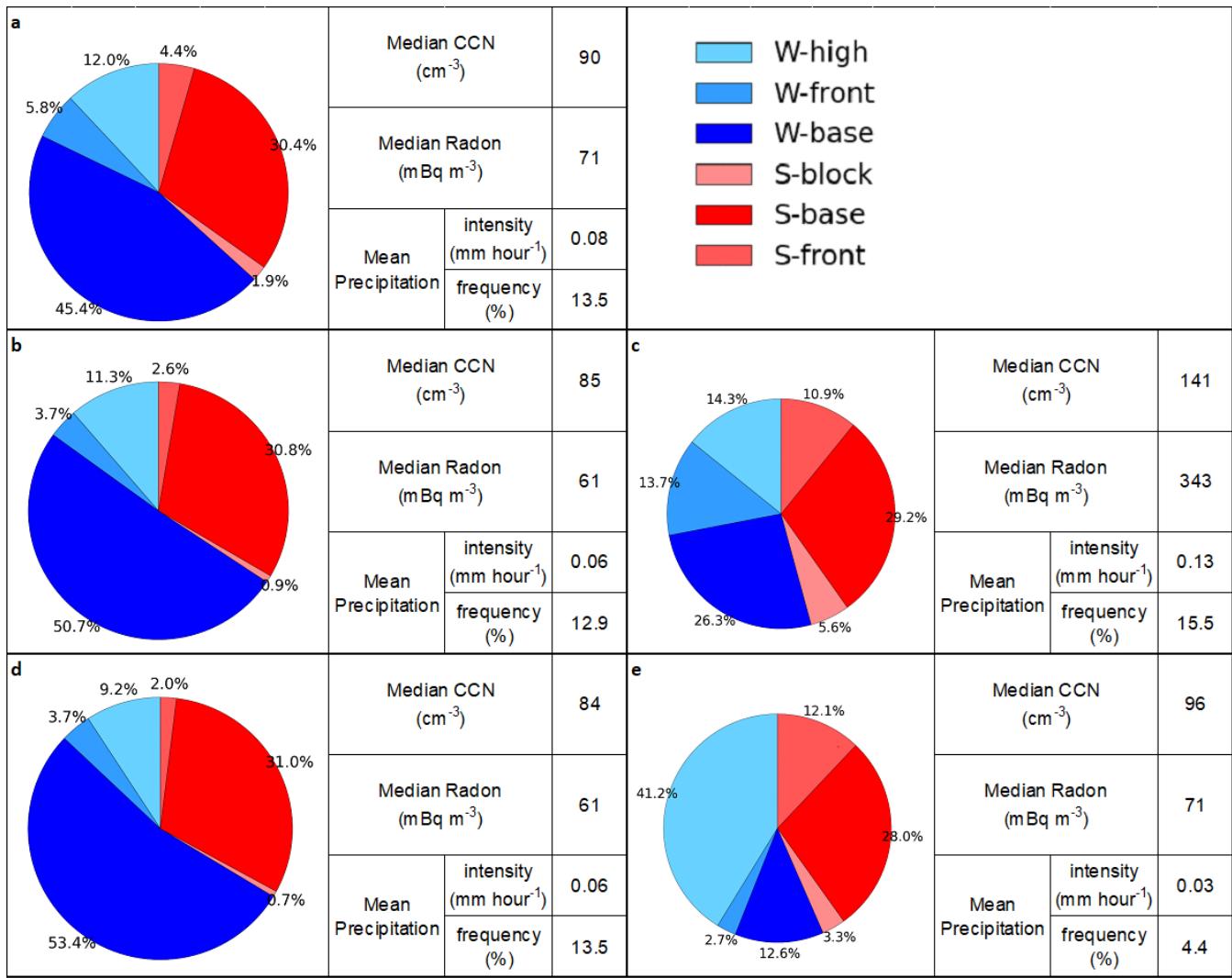
Figure 7. Comparison of derived clusters with CGO baseline criteria using three criteria: (a) wind direction (190°-280°), (b) wind direction plus radon <150 mBq m^{-3}, (c) cases removed when adding radon criterion to (a), (d) wind direction and radon plus wind speed >5 m s^{-1} and (e) cases removed when adding wind speed criterion to (b).

A third criterion based on wind speed can be further applied to the CGO baseline definition. Following the literature, we set a minimum wind speed of 5 m s^{-1} (Jimi et al., 2007), which removes a further 7% of the record. W-base and S-base comprise nearly 85% of these remaining records. Both CCN and radon concentration do not show changes by this last constraint (Figure 7d). Not surprisingly, W-high records, which have low surface wind speeds, are primarily removed by this last constraint (Figure7e). Nevertheless, over 9% of this highly constrained CGO baseline record still come from W-high rather than baseline clusters.

It is interesting to directly compare efficiency of the two different methods of defining baseline conditions. The most constrained CGO definition, using all three thresholds, produces a median value of 84 cm^{-3} for N_{CCN} and 61 mBq m^{-3} for radon. This method makes no distinction for winter or summer. Conversely the original W-base cluster produced values of 71 cm^{-3} and 66 mBq m^{-3} for N_{CCN} and radon, respectively, while the S-base cluster produced values of 137 cm^{-3} and 80 mBq m^{-3} (Table 1). This again suggests that the seasonal changes in the meteorology are having a direct effect on the seasonal cycle of N_{CCN} as observed at CGO.

6 Discussion and Conclusion

Our study provides new insight into the impact that the synoptic meteorology has on the observed seasonality in N_{CCN} at CGO. Specifically, we explore how the seasonality of the synoptic meteorology affects precipitation, which acts as a sink through wet deposition, and the free troposphere transport of terrestrial air masses, which acts as a source of N_{CCN} through entrainment.

Utilizing clustering analysis on ERA5 thermodynamic data, we observed a strong seasonal cycle in the synoptic meteorology. Specifically, three synoptic clusters (W-base, W-front and W-high) were found to be more prevalent during the winter months (JJA) while another three (S-base, S-front and S-block) were more common in summertime (DJF). The baseline clusters, W-base and S-base, are characterized by south westerly winds at the surface, with a deeper boundary layer inversion in winter suggesting more frequent precipitation from shallow MABL clouds. The frontal clusters, W-front and S-front, feature strong north westerly winds through the free troposphere, with W-front exhibiting higher relative humidity. W-high displays near zero wind speed, on average, and minimal precipitation, while S-block is characterized by low wind speed, anti-cyclonic atmospheric conditions.

Not surprisingly, the W-base cluster is characterized as the most pristine air mass, while S-base, which occasionally passes over Australia, exhibits around twice the concentration of CCN and 20% higher radon concentration. These findings highlight a large seasonal cycle in N_{CCN} consistent with previous research (Ayers et al., 1997; Gras and Keywood, 2017; Humphries et al., 2023). Conversely, the two frontal clusters are identified as the least pristine, with N_{CCN} more than three times greater than the corresponding baseline clusters. The two remaining clusters, W-high and S-block, fall between the extremes. Overall, the combined summer clusters (S-base, S-front and S-block) exhibit higher CCN and radon concentrations than the combined winter clusters (W-base, W-front and W-high).

Our analysis reveals an inverse relationship between precipitation and N_{CCN} during both the baseline and frontal clusters, highlighting the role of coalescence scavenging and wet deposition in cleansing the atmosphere and reducing N_{CCN} over the SO (Kang et al., 2022; Sanchez et al., 2021; Alinejdtabrizi et al., 2024).

Our analysis of the role of free troposphere entrainment at CGO was inconclusive. While the back trajectory analysis reveals that S-base is more commonly affected by terrestrial (Australia) influences, it was not possible to isolate free troposphere entrainment of N_{CCN} from direct surface emissions. Either way, however, the S-base air mass is more frequently affected by

390 terrestrial sources than the W-base air masses, again revealing that other sources are contributing to the seasonal cycle in N_{CCN} as observed at CGO other than biogenic production.

On average the characteristics of our two baseline clusters are consistent with those of the traditional CGO baseline air mass. Our analysis finds that the wintertime baseline precipitation is approximately three times greater than that during the summer, helping make the wintertime baseline air mass more 'pristine' through wet deposition. An examination of the transport of

395 the overlying free troposphere air also finds a distinct seasonal cycle with terrestrial air masses more commonly passing over kennaook/Cape Grim during the summer season, when the subtropical ridge is furthest poleward. The entrainment of this terrestrial free troposphere air into the boundary layer will also contribute to seasonal cycle in N_{CCN}.

Our analysis of back trajectories reveals that overall, during the winter, when the STR resides further north, toward the equator, CGO exhibits heightened connectivity to the higher latitudes and Antarctica. Conversely, during summer when the STR

400 shifts poleward, this connectivity is weakened. In effect, the STR acts as a barrier. This seasonal modulation underscores the significant influence of large-scale meteorological patterns on air mass observed at CGO.

With respect to our understanding of the CGO baseline air mass, two salient points arise. First, the current criteria for defining the CGO baseline air mass includes a non-negligible percentage from the W-high synoptic class. Second, and more importantly, there are significant seasonal differences in the boundary layer structure, precipitation and air mass origin (both boundary layer

405 and free troposphere). Echoing the conclusions of Quinn and Bates (2011), a full understanding of the N_{CCN} budget over the SO is far more complex than simply an understanding of the biogenic production. In particular, it is essential to understand the role of precipitation from shallow convection across the SO (Siems et al., 2022; Alinejadtabrizi et al., 2024).

Data availability. The N_{CCN} measurement, analyzed during the current study are available in the World Data Centre for Aerosols [http://www.gaw-wdca.org/]. The ECMWF-ERA5 reanalysis datasets are available through the Copernicus Climate Change Service Climate Data Store

410 [https://cds.climate.copernicus.eu]. The precipitation data can be obtained by contacting [climatedata@bom.gov.au]. The radon data is available from the World Data Centre for Greenhouse Gases (WDCGG) [https://gaw.kishou.go.jp/] and from Alastair Williams from Australian Nuclear Science and Technology Organisation (ANSTO).

Appendix A: Evidence of the subsidence over the CGO
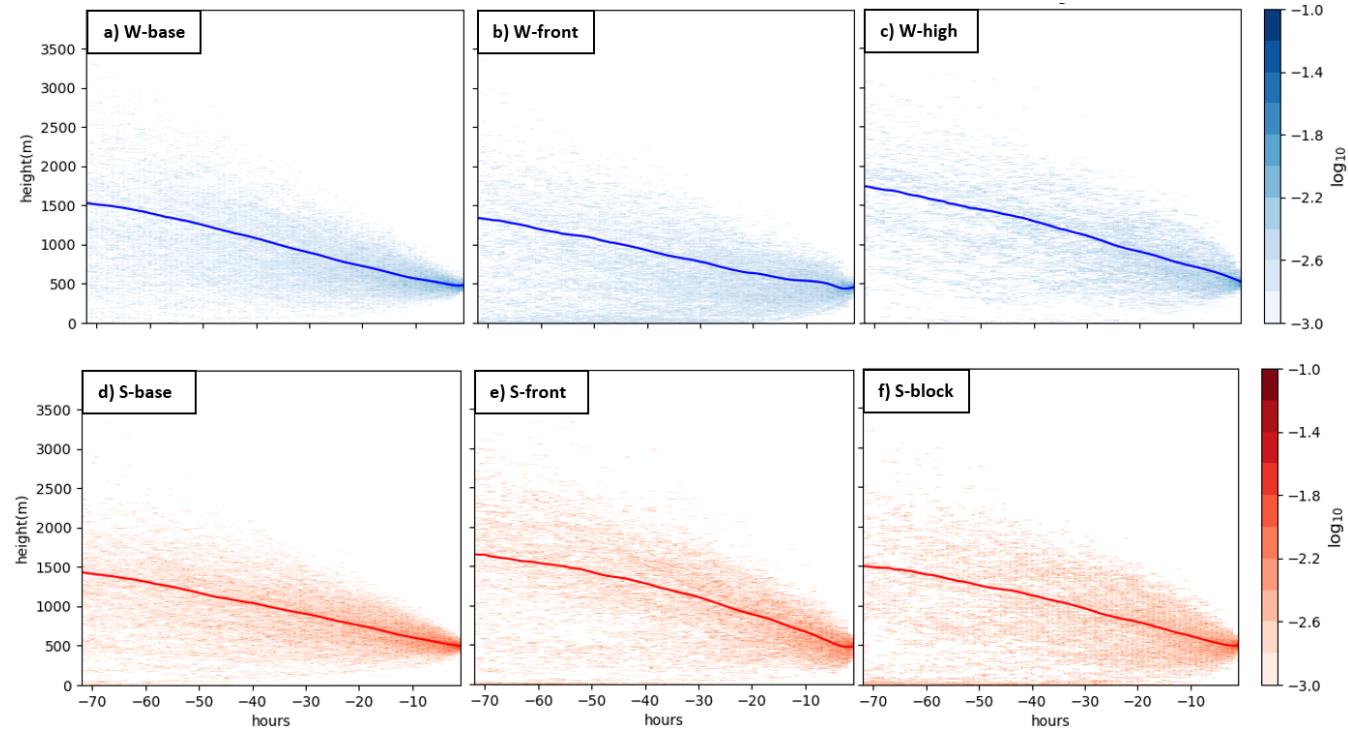
Figure A1. Frequency of the height distribution of 72 hours back trajectories at 500 m (boundary layer) level with the average as a solid line, for six clusters (2011-2021).

Appendix B: Further environmental context for each cluster

Table B1. Mean inversion height (hPa), TCWV (mm) and EIS (°K) for each cluster.

Cluster	Inversion Height (hPa)	TCWV (mm)	EIS (°K)
W-base	850	13.1	4.3
S-base	900	16.9	6.6
W-front	-[*]	19.6	1.2
S-front	-[*]	21.9	3.9
W-high	900	12.1	6.3
S-block	950	20.0	4.7

[*] There is no clear inversion for the frontal systems.

415 *Author contributions.* Alinejadtabrizi performed the data analysis and prepared the original draft of the paper. All co-authors provided editorial feedback on the paper. All co-authors read and approved the final manuscript.

Competing interests. At least one of the (co-)authors is a member of the editorial board of Atmospheric Chemistry and Physics. Authors have no other competing interests to declare

Acknowledgements. This research has been supported by Securing Antarctica's Environmental Future (SAEF), a Special Research Initiative
420 of the Australian Research Council (SRI20010005) and also by the Australian Research Council (ARC) Centre of Excellence for Climate Extremes (CE170100023) and the ARC Discovery Projects (DP190101362). Continued support for the kennaook Cape Grim Program from the Australian Bureau of Meteorology and Commonwealth Scientific and Industrial Research Organisation (CSIRO) is also gratefully acknowledged.

References

425 Ahn, E., Huang, Y., Chubb, T. H., Baumgardner, D., Isaac, P., de Hoog, M., Siems, S. T., and Manton, M. J.: In situ observations of wintertime low-altitude clouds over the Southern Ocean, Quarterly Journal of the Royal Meteorological Society, 143, 1381–1394, 2017.

Alinejadtabrizi, T., Lang, F., Huang, Y., Ackermann, L., Keywood, M., Ayers, G., Krummel, P., Humphries, R., Williams, A., and Siems, S.: Wet deposition in shallow convection over the Southern Ocean, npj Climate and Atmospheric Science, 7, 76, 2024.

Anderberg, M. R.: Cluster Analysis for Applications, 1973.

430 Ayers, G. and Gillett, R.: DMS and its oxidation products in the remote marine atmosphere: implications for climate and atmospheric chemistry, Journal of Sea Research, 43, 275–286, 2000.

Ayers, G., Bigg, E., Turvey, D., and Manton, M.: Urban influence on condensation nuclei over a continent, Atmospheric Environment (1967), 16, 951–954, 1982.

Ayers, G., Bentley, S., Ivey, J., and Forgan, B.: Dimethylsulfide in marine air at Cape Grim, 41 S, Journal of Geophysical Research: Atmo-
435   spheres, 100, 21 013–21 021, 1995.

Ayers, G. P. and Cainey, J. M.: The CLAW hypothesis: a review of the major developments, Environmental Chemistry, 4, 366–374, 2007.

Ayers, G. P., Cainey, J. M., Gillett, R., and Ivey, J. P.: Atmospheric sulphur and cloud condensation nuclei in marine air in the Southern Hemisphere, Philosophical Transactions of the Royal Society of London. Series B: Biological Sciences, 352, 203–211, 1997.

Bates, T. S., Huebert, B. J., Gras, J. L., Griffiths, F. B., and Durkee, P. A.: International Global Atmospheric Chemistry (IGAC) project's first
440   aerosol characterization experiment (ACE 1): Overview, Journal of Geophysical Research: Atmospheres, 103, 16 297–16 318, 1998.

Bigg, E., Gras, J., and Evans, C.: Origin of Aitken particles in remote regions of the Southern Hemisphere, Journal of atmospheric chemistry, 1, 203–214, 1984.

Bodas-Salcedo, A., Williams, K. D., Ringer, M. A., Beau, I., Cole, J. N., Dufresne, J.-L., Koshiro, T., Stevens, B., Wang, Z., and Yokohata, T.: Origins of the solar radiation biases over the Southern Ocean in CFMIP2 models, Journal of Climate, 27, 41–56, 2014.

445 Boers, R., Jensen, J., and Krummel, P.: Microphysical and short-wave radiative structure of stratocumulus clouds over the Southern Ocean: Summer results and seasonal differences, Quarterly Journal of the Royal Meteorological Society, 124, 151–168, 1998.

Cai, W., Van Rensch, P., and Cowan, T.: Influence of global-scale variability on the subtropical ridge over southeast Australia, Journal of Climate, 24, 6035–6053, 2011.

Capaldo, K. P., Kasibhatla, P., and Pandis, S. N.: Is aerosol production within the remote marine boundary layer sufficient to maintain
450   observed concentrations?, Journal of Geophysical Research: Atmospheres, 104, 3483–3500, 1999.

Chambers, S. D., Williams, A. G., Crawford, J., and Griffiths, A. D.: On the use of radon for quantifying the effects of atmospheric stability on urban emissions, Atmos. Chem. Phys., 15, 1175–1190, https://doi.org/10.5194/acp-15-1175-2015, 2015.

Chambers, S. D., Preunkert, S., Weller, R., Hong, S.-B., Humphries, R. S., Tositti, L., Angot, H., Legrand, M., Williams, A. G., Griffiths, A. D., Crawford, J., Simmons, J., Choi, T. J., Krummel, P. B., Molloy, S., Loh, Z., Galbally, I., Wilson, S., Magand, O., Sprovieri, F.,
455   Pirrone, N., and Dommergue, A.: Characterizing Atmospheric Transport Pathways to Antarctica and the Remote Southern Ocean Using Radon-222, Frontiers in Earth Science, 6, https://doi.org/10.3389/feart.2018.00190, 2018.

Charlson, R. J., Lovelock, J. E., Andreae, M. O., and Warren, S. G.: Oceanic phytoplankton, atmospheric sulphur, cloud albedo and climate, Nature, 326, 655–661, 1987.

Clarke, A., Varner, J., Eisele, F., Mauldin, R., Tanner, D., and Litchy, M.: Particle production in the remote marine atmosphere: Cloud outflow
460   and subsidence during ACE 1, Journal of Geophysical Research: Atmospheres, 103, 16 397–16 409, 1998.

Covert, D. S., Kapustin, V. N., Bates, T. S., and Quinn, P. K.: Physical properties of marine boundary layer aerosol particles of the mid-Pacific in relation to sources and meteorological transport, Journal of Geophysical Research: Atmospheres, 101, 6919–6930, https://doi.org/https://doi.org/10.1029/95JD03068, 1996.

465 Danker, J., Sourdeval, O., McCoy, I. L., Wood, R., and Possner, A.: Exploring relations between cloud morphology, cloud phase, and cloud radiative properties in Southern Ocean's stratocumulus clouds, Atmospheric Chemistry and Physics, 22, 10 247–10 265, 2022.

Dima, I. M. and Wallace, J. M.: On the seasonality of the Hadley cell, Journal of the atmospheric sciences, 60, 1522–1527, 2003.

Draxler, R. R. and Hess, G. D.: An overview of the HYSPLIT$_4$ $modeling system for trajectories, dispersion, and deposition, Aust. Meteor. Mag., 47$ $-308, 1998.$

Feingold, G., Kreidenweis, S. M., Stevens, B., and Cotton, W.: Numerical simulations of stratocumulus processing of cloud condensation nuclei through collision-coalescence, Journal of Geophysical Research: Atmospheres, 101, 21 391–21 402, 1996.

Fletcher, J. K., Mason, S., and Jakob, C.: A Climatology of Clouds in Marine Cold Air Outbreaks in Both Hemispheres, Journal of Climate, 29,
470 6677–6692, https://doi.org/https://doi.org/10.1175/JCLI-D-15-0783.1, 2016.

Forbes, R. M. and Ahlgrimm, M.: On the Representation of High-Latitude Boundary Layer Mixed-Phase Cloud in the ECMWF Global Model, Monthly Weather Review, 142, 3425–3445, https://doi.org/https://doi.org/10.1175/MWR-D-13-00325.1, 2014.

Fossum, K. N., Ovadnevaite, J., Ceburnis, D., Dall'Osto, M., Marullo, S., Bellacicco, M., Simó, R., Liu, D., Flynn, M., Zuend, A., and O'Dowd, C.: Summertime Primary and Secondary Contributions to Southern Ocean Cloud Condensation Nuclei, Scientific Reports, 8,
475 13 844, https://doi.org/10.1038/s41598-018-32047-4, 2018.

Gordon, N. D. and Norris, J. R.: Cluster analysis of midlatitude oceanic cloud regimes: mean properties and temperature sensitivity, Atmos. Chem. Phys., 10, 6435–6459, https://doi.org/10.5194/acp-10-6435-2010, 2010.

Gras, J.: CN, CCN and particle size in Southern Ocean air at Cape Grim, Atmospheric research, 35, 233–251, 1995.

Gras, J. L.: Cloud condensation nuclei over the Southern Ocean, Geophysical research letters, 17, 1565–1567, 1990.

480 Gras, J. L. and Keywood, M.: Cloud condensation nuclei over the Southern Ocean: wind dependence and seasonal cycles, Atmospheric Chemistry and Physics, 17, 4419–4432, 2017.

Gras, J. L., Jimi, S. I., Siems, S. T., and Krummel, P. B.: Postfrontal nanoparticles at Cape Grim: observations, Environmental Chemistry, 6, 508–514, https://doi.org/https://doi.org/10.1071/EN09075, 2009.

Grose, M., Timbal, B., Wilson, L., Bathols, J., and Kent, D.: The subtropical ridge in CMIP5 models, and implications for projections of rainfall
485 in southeast Australia, Australian Meteorological and Oceanographic Journal, 65, 90–106, https://doi.org/https://doi.org/10.1071/ES15007, 2015.

Hande, L. B., Siems, S. T., and Manton, M. J.: Observed Trends in Wind Speed over the Southern Ocean, Geophysical Research Letters, 39, https://doi.org/https://doi.org/10.1029/2012GL051734, 2012.

Haynes, J. M., Jakob, C., Rossow, W. B., Tselioudis, G., and Brown, J.: Major Characteristics of Southern Ocean Cloud Regimes and Their
490 Effects on the Energy Budget, Journal of Climate, 24, 5061–5080, https://doi.org/https://doi.org/10.1175/2011JCLI4052.1, 2011.

Hersbach, H., Bell, B., Berrisford, P., Hirahara, S., Horányi, A., Muñoz-Sabater, J., Nicolas, J., Peubey, C., Radu, R., Schepers, D., Simmons, A., Soci, C., Abdalla, S., Abellan, X., Balsamo, G., Bechtold, P., Biavati, G., Bidlot, J., Bonavita, M., De Chiara, G., Dahlgren, P., Dee, D., Diamantakis, M., Dragani, R., Flemming, J., Forbes, R., Fuentes, M., Geer, A., Haimberger, L., Healy, S., Hogan, R. J., Hólm, E., Janisková, M., Keeley, S., Laloyaux, P., Lopez, P., Lupu, C., Radnoti, G., de Rosnay, P., Rozum, I., Vamborg, F., Villaume, S., and Thépaut, J.-N.: The ERA5
495 global reanalysis, Quarterly Journal of the Royal Meteorological Society, 146, 1999–2049, https://doi.org/https://doi.org/10.1002/qj.3803, 2020.

Huang, Y., Protat, A., Siems, S. T., and Manton, M. J.: A-Train observations of maritime midlatitude storm-track cloud systems: Comparing the Southern Ocean against the North Atlantic, Journal of Climate, 28, 1920–1939, 2015.

Hudson, J. G., Noble, S., and Jha, V.: On the relative role of sea salt cloud condensation nuclei (CCN), Journal of atmospheric chemistry, 68, 71–88, 2011.

Humphries, R. S., Keywood, M. D., Gribben, S., McRobert, I. M., Ward, J. P., Selleck, P., Taylor, S., Harnwell, J., Flynn, C., and Kulkarni, G. R.: Southern Ocean latitudinal gradients of cloud condensation nuclei, Atmospheric Chemistry and Physics, 21, 12 757–12 782, 2021.

Humphries, R. S., Keywood, M. D., Ward, J. P., Harnwell, J., Alexander, S. P., Klekociuk, A. R., Hara, K., McRobert, I. M., Protat, A., and Alroe, J.: Measurement report: Understanding the seasonal cycle of Southern Ocean aerosols, Atmospheric Chemistry and Physics, 23, 3749–3777, 2023.

Jimi, S. I., Gras, J., Siems, S. T., and Krummel, P. B.: A short climatology of nanoparticles at the Cape Grim Baseline Air Pollution Station, Tasmania, Environmental Chemistry, 4, 301–309, https://doi.org/https://doi.org/10.1071/EN07038, 2007.

Kang, L., Marchand, R., Wood, R., and McCoy, I. L.: Coalescence scavenging drives droplet number concentration in southern ocean low clouds, Geophysical Research Letters, 49, e2022GL097 819, 2022.

Katoshevski, D., Nenes, A., and Seinfeld, J. H.: A study of processes that govern the maintenance of aerosols in the marine boundary layer, Journal of Aerosol Science, 30, 503–532, 1999.

Kay, J. E., Wall, C., Yettella, V., Medeiros, B., Hannay, C., Caldwell, P., and Bitz, C.: Global Climate Impacts of Fixing the Southern Ocean Shortwave Radiation Bias in the Community Earth System Model (CESM), Journal of Climate, 29, 4617–4636, https://doi.org/https://doi.org/10.1175/JCLI-D-15-0358.1, 2016.

Klein, S. A. and Hartmann, D. L.: The seasonal cycle of low stratiform clouds, Journal of Climate, 6, 1587–1606, 1993.

Korhonen, H., Carslaw, K. S., Spracklen, D. V., Mann, G. W., and Woodhouse, M. T.: Influence of oceanic dimethyl sulfide emissions on cloud condensation nuclei concentrations and seasonality over the remote Southern Hemisphere oceans: A global model study, Journal of Geophysical Research: Atmospheres, 113, 2008.

Lang, F., Huang, Y., Siems, S. T., and Manton, M. J.: Characteristics of the Marine Atmospheric Boundary Layer Over the Southern Ocean in Response to the Synoptic Forcing, Journal of Geophysical Research: Atmospheres, 123, 7799–7820, https://doi.org/https://doi.org/10.1029/2018JD028700, 2018.

Lang, F., Ackermann, L., Huang, Y., Truong, S. C., Siems, S. T., and Manton, M. J.: A climatology of open and closed mesoscale cellular convection over the Southern Ocean derived from Himawari-8 observations, Atmospheric Chemistry and Physics, 22, 2135–2152, 2022.

Lang, F., Siems, S. T., Huang, Y., Alinejadtabrizi, T., and Ackermann, L.: On the relationship between mesoscale cellular convection and meteorological forcing: comparing the Southern Ocean against the North Pacific, Atmos. Chem. Phys., 24, 1451–1466, https://doi.org/10.5194/acp-24-1451-2024, 2024.

Larsen, S. H. and Nicholls, N.: Southern Australian rainfall and the subtropical ridge: Variations, interrelationships, and trends, Geophysical Research Letters, 36, 2009.

Mace, G. G. and Avey, S.: Seasonal variability of warm boundary layer cloud and precipitation properties in the Southern Ocean as diagnosed from A-Train data, Journal of Geophysical Research: Atmospheres, 122, 1015–1032, https://doi.org/https://doi.org/10.1002/2016JD025348, 2017.

Manton, M. J., Huang, Y., and Siems, S. T.: Variations in Precipitation across the Southern Ocean, Journal of Climate, 33, 10 653–10 670, https://doi.org/https://doi.org/10.1175/JCLI-D-20-0120.1, 2020.

Mason, S., Jakob, C., Protat, A., and Delanoë, J.: Characterizing observed midtopped cloud regimes associated with Southern Ocean shortwave radiation biases, Journal of climate, 27, 6189–6203, 2014.

McCoy, D. T., Hartmann, D. L., and Grosvenor, D. P.: Observed Southern Ocean Cloud Properties and Shortwave Reflection. Part I: Calculation of SW Flux from Observed Cloud Properties, Journal of Climate, 27, 8836–8857, https://doi.org/https://doi.org/10.1175/JCLI-D-14-00287.1, 2014.

McCoy, D. T., Burrows, S. M., Wood, R., Grosvenor, D. P., Elliott, S. M., Ma, P.-L., Rasch, P. J., and Hartmann, D. L.: Natural aerosols explain seasonal and spatial patterns of Southern Ocean cloud albedo, Science advances, 1, e1500 157, 2015.

McCoy, I. L., Wood, R., and Fletcher, J. K.: Identifying meteorological controls on open and closed mesoscale cellular convection associated with marine cold air outbreaks, Journal of Geophysical Research: Atmospheres, 122, 11,678–11,702, 2017.

McFarquhar, G. M., Bretherton, C. S., Marchand, R., Protat, A., DeMott, P. J., Alexander, S. P., Roberts, G. C., Twohy, C. H., Toohey, D., and Siems, S.: Observations of clouds, aerosols, precipitation, and surface radiation over the Southern Ocean: An overview of CAPRICORN, MARCUS, MICRE, and SOCRATES, Bulletin of the American Meteorological Society, 102, E894–E928, 2021.

Mechem, D. B., Robinson, P. C., and Kogan, Y. L.: Processing of cloud condensation nuclei by collision-coalescence in a mesoscale model, Journal of Geophysical Research: Atmospheres, 111, 2006.

Montoya Duque, E., Huang, Y., Siems, S. T., May, P. T., Protat, A., and McFarquhar, G. M.: A Characterization of Clouds and Precipitation Over the Southern Ocean From Synoptic to Micro Scales During the CAPRICORN Field Campaigns, Journal of Geophysical Research: Atmospheres, 127, e2022JD036 796, https://doi.org/https://doi.org/10.1029/2022JD036796, 2022.

Montoya Duque, E., Huang, Y., May, P. T., and Siems, S. T.: An Evaluation of IMERG and ERA5 Quantitative Precipitation Estimates over the Southern Ocean Using Shipborne Observations, Journal of Applied Meteorology and Climatology, 62, 1479–1495, https://doi.org/https://doi.org/10.1175/JAMC-D-23-0039.1, 2023.

Niu, Q., McFarquhar, G. M., Marchand, R., Theisen, A., Cavallo, S. M., Flynn, C., DeMott, P. J., McCluskey, C. S., Humphries, R. S., and Hill, T. C. J.: 62°S Witnesses the Transition of Boundary Layer Marine Aerosol Pattern Over the Southern Ocean (50°S–68°S, 63°E–150°E) During the Spring and Summer: Results From MARCUS (I), Journal of Geophysical Research: Atmospheres, 129, e2023JD040 396, https://doi.org/https://doi.org/10.1029/2023JD040396, 2024.

Painemal, D., Chellappan, S., Smith Jr., W. L., Spangenberg, D., Park, J. M., Ackerman, A., Chen, J., Crosbie, E., Ferrare, R., Hair, J., Kirschler, S., Li, X.-Y., McComiskey, A., Moore, R. H., Sanchez, K., Sorooshian, A., Tornow, F., Voigt, C., Wang, H., Winstead, E., Zeng, X., Ziemba, L., and Zuidema, P.: Wintertime Synoptic Patterns of Midlatitude Boundary Layer Clouds Over the Western North Atlantic: Climatology and Insights From In Situ ACTIVATE Observations, Journal of Geophysical Research: Atmospheres, 128, e2022JD037 725, https://doi.org/https://doi.org/10.1029/2022JD037725, 2023.

Pepler, A., Ashcroft, L., and Trewin, B.: The relationship between the subtropical ridge and Australian temperatures, Journal of Southern Hemisphere Earth Systems Science, 68, 201–214, https://doi.org/https://doi.org/10.1071/ES18011, 2018.

Pittock, A.: Global meridional interactions in stratosphere and troposphere, Quarterly Journal of the Royal Meteorological Society, 99, 424–437, 1973.

Quinn, P. K. and Bates, T. S.: The case against climate regulation via oceanic phytoplankton sulphur emissions, Nature, 480, 51–56, 2011.

Quinn, P. K., Bates, T. S., Schulz, K. S., Coffman, D., Frossard, A., Russell, L., Keene, W., and Kieber, D.: Contribution of sea surface carbon pool to organic matter enrichment in sea spray aerosol, Nature Geoscience, 7, 228–232, 2014.

570 Redemann, J., Wood, R., Zuidema, P., Doherty, S. J., Luna, B., LeBlanc, S. E., Diamond, M. S., Shinozuka, Y., Chang, I. Y., and Ueyama, R.: An overview of the ORACLES (ObseRvations of Aerosols above CLouds and their intEractionS) project: aerosol-cloud-radiation interactions in the Southeast Atlantic basin, Atmospheric Chemistry and Physics Discussions, 2020, 1–82, 2020.

Risbey, J. S., Pook, M. J., and McIntosh, P. C.: Spatial trends in synoptic rainfall in southern Australia, Geophysical Research Letters, 40, 3781–3785, https://doi.org/https://doi.org/10.1002/grl.50739, 2013.

575 Rose, C., Sellegri, K., Moreno, I., Velarde, F., Ramonet, M., Weinhold, K., Krejci, R., Andrade, M., Wiedensohler, A., and Ginot, P.: CCN production by new particle formation in the free troposphere, Atmospheric Chemistry and Physics, 17, 1529–1541, 2017.

Sanchez, K. J., Chen, C.-L., Russell, L. M., Betha, R., Liu, J., Price, D. J., Massoli, P., Ziemba, L. D., Crosbie, E. C., and Moore, R. H.: Substantial seasonal contribution of observed biogenic sulfate particles to cloud condensation nuclei, Scientific reports, 8, 3235, 2018.

Sanchez, K. J., Roberts, G. C., Saliba, G., Russell, L. M., Twohy, C., Reeves, J. M., Humphries, R. S., Keywood, M. D., Ward, J. P., and
580 McRobert, I. M.: Measurement report: Cloud processes and the transport of biological emissions affect southern ocean particle and cloud condensation nuclei concentrations, Atmospheric Chemistry and Physics, 21, 3427–3446, 2021.

Schuddeboom, A. and McDonald, A.: The Southern Ocean radiative bias, cloud compensating errors, and equilibrium climate sensitivity in CMIP6 models, Journal of Geophysical Research: Atmospheres, 126, e2021JD035 310, 2021.

Siems, S. T., Huang, Y., and Manton, M. J.: Southern Ocean precipitation: Toward a process-level understanding, WIREs Climate Change, 13,
585 e800, https://doi.org/https://doi.org/10.1002/wcc.800, 2022.

Tan, I., Storelvmo, T., and Zelinka, M. D.: Observational constraints on mixed-phase clouds imply higher climate sensitivity, Science, 352, 224–227, 2016.

Trenberth, K. E. and Fasullo, J. T.: Simulation of present-day and twenty-first-century energy budgets of the southern oceans, Journal of Climate, 23, 440–454, 2010.

590 Truong, S. C. H., Huang, Y., Lang, F., Messmer, M., Simmonds, I., Siems, S. T., and Manton, M. J.: A Climatology of the Marine Atmospheric Boundary Layer Over the Southern Ocean From Four Field Campaigns During 2016–2018, Journal of Geophysical Research: Atmospheres, 125, e2020JD033 214, https://doi.org/https://doi.org/10.1029/2020JD033214, 2020.

Truong, S. C. H., Huang, Y., Siems, S. T., Manton, M. J., and Lang, F.: Biases in the thermodynamic structure over the Southern Ocean in ERA5 and their radiative implications, Int. J. Climatol., 42, 7685–7702, 2022.

595 Twohy, C. H., DeMott, P. J., Russell, L. M., Toohey, D. W., Rainwater, B., Geiss, R., Sanchez, K. J., Lewis, S., Roberts, G. C., and Humphries, R. S.: Cloud-nucleating particles over the Southern Ocean in a changing climate, Earth's Future, 9, e2020EF001 673, 2021.

Vallina, S. M., Simó, R., and Gassó, S.: What controls CCN seasonality in the Southern Ocean? A statistical analysis based on satellite-derived chlorophyll and CCN and model-estimated OH radical and rainfall, Global Biogeochemical Cycles, 20, 2006.

Whittlestone, S. and Zahorowski, W.: Baseline radon detectors for shipboard use: Development and deployment in the
600 First Aerosol Characterization Experiment (ACE 1), Journal of Geophysical Research: Atmospheres, 103, 16 743–16 751, https://doi.org/https://doi.org/10.1029/98JD00687, 1998.

Williams, A. and Chambers, S.: A history of radon measurements at Cape Grim, Baseline Atmospheric Program (Australia) History and Recollections, 40th Anniversary Special edn, pp. 131–146, 2016.

Williams, A. A. J. and Stone, R. C.: An assessment of relationships between the Australian subtropical ridge, rainfall variability, and high-
605 latitude circulation patterns, International Journal of Climatology, 29, 691–709, https://doi.org/https://doi.org/10.1002/joc.1732, 2009.

Williams, K. D., Bodas-Salcedo, A., Déqué, M., Fermepin, S., Medeiros, B., Watanabe, M., Jakob, C., Klein, S. A., Senior, C. A., and Williamson, D. L.: The Transpose-AMIP II experiment and its application to the understanding of Southern Ocean cloud biases in climate models, Journal of Climate, 26, 3258–3274, 2013.

Williamson, C. J., Kupc, A., Axisa, D., Bilsback, K. R., Bui, T., Campuzano-Jost, P., Dollner, M., Froyd, K. D., Hodshire, A. L., Jimenez, J. L.,
610   Kodros, J. K., Luo, G., Murphy, D. M., Nault, B. A., Ray, E. A., Weinzierl, B., Wilson, J. C., Yu, F., Yu, P., Pierce, J. R., and Brock, C. A.: A large source of cloud condensation nuclei from new particle formation in the tropics, Nature, 574, 399–403, https://doi.org/10.1038/s41586-019-1638-9, 2019.

Wood, R.: Rate of loss of cloud droplets by coalescence in warm clouds, Journal of Geophysical Research: Atmospheres, 111, 2006.

Wood, R.: Stratocumulus clouds, Monthly weather review, 140, 2373–2423, 2012.

615 Wood, R. and Bretherton, C. S.: On the Relationship between Stratiform Low Cloud Cover and Lower-Tropospheric Stability, Journal of Climate, 19, 6425–6432, https://doi.org/https://doi.org/10.1175/JCLI3988.1, 2006.

Wood, R., Leon, D., Lebsock, M., Snider, J., and Clarke, A. D.: Precipitation driving of droplet concentration variability in marine low clouds, Journal of Geophysical Research: Atmospheres, 117, 2012.

Zahorowski, W., Griffiths, A. D., Chambers, S. D., Williams, A. G., Law, R. M., Crawford, J., and Werczynski, S.: Constraining annual and
620   seasonal radon-222 flux density from the Southern Ocean using radon-222 concentrations in the boundary layer at Cape Grim, Tellus B: Chemical and Physical Meteorology, 65, 19 622, https://doi.org/10.3402/tellusb.v65i0.19622, 2013.

Zelinka, M. D., Myers, T. A., McCoy, D. T., Po-Chedley, S., Caldwell, P. M., Ceppi, P., Klein, S. A., and Taylor, K. E.: Causes of higher climate sensitivity in CMIP6 models, Geophysical Research Letters, 47, e2019GL085 782, 2020.